Title
Fully coupled simulation of the plasma liquid interface and interfacial coefficient effects

Journal
Journal of Physics D, 49(23)

ISSN
0022-3727

Authors
Lindsay, Alexander D
Graves, David B
Shannon, Steven C

Publication Date
2016-06-15

DOI
10.1088/0022-3727/49/23/235204

Peer reviewed

Fully coupled simulation of the plasma liquid interface and interfacial coefficient effects

IOP Publishing Journal of Physics D: Applied Physics

J. Phys. D: Appl. Phys. **49** (2016) 235204 (9pp) doi:10.1088/0022-3727/49/23/235204

Fully coupled simulation of the plasma liquid interface and interfacial coefficient effects

Alexander D Lindsay[1], David B Graves[2] and Steven C Shannon[1]

[1] North Carolina State University, Nuclear Engineering Department, Raleigh NC, USA
[2] University of California-Berkeley, Chemical Engineering Department, CA, USA

E-mail: adlinds3@ncsu.edu

Received 4 March 2016, revised 5 April 2016
Accepted for publication 8 April 2016
Published 6 May 2016

Abstract

There is a growing interest in the study of coupled plasma-liquid systems because of their applications to biomedicine, biological and chemical disinfection, agriculture, and other areas. Optimizing these applications requires a fundamental understanding of the coupling between phases. Though much progress has been made in this regard, there is still more to be done. One area that requires more research is the transport of electrons across the plasma-liquid interface. Some pioneering works (Rumbach *et al* 2015 *Nat. Commun.* **6**, Rumbach *et al* 2015 *J. Phys. D: Appl. Phys.* **48** 424001) have begun revealing the near-surface liquid characteristics of electrons. However, there has been little work to determine the near-surface gas phase electron characteristics. Without an understanding of the near-surface gas dynamics, modellers are left to make assumptions about the interfacial conditions. For instance it is commonly assumed that the surface loss or sticking coefficient of gas-phase electrons at the interface is equal to 1. In this work we explore the consequences of this assumption and introduce a couple of ways to think about the electron interfacial condition. In one set of simulations we impose a kinetic condition with varying surface loss coefficient on the gas phase interfacial electrons. In a second set of simulations we introduce a Henry's law like condition at the interface in which the gas-phase electron concentration is assumed to be in thermodynamic equilibrium with the liquid-phase electron concentration. It is shown that for a range of electron Henry coefficients spanning a range of known hydrophilic specie Henry coefficients, the gas phase electron density in the anode can vary by orders of magnitude. Varying reflection of electrons by the interface also has consequences for the electron energy profile; increasing reflection may lead to increasing thermalization of electrons depending on choices about the electron energy boundary condition. This variation in anode electron density and energy as a function of the interface characteristics could also lead to significant variation in near-surface gas chemistries when such reactions are included in the model; this could very well in turn affect the reactive species impinging on the liquid surface. We draw the conclusion that in order to make more confident model predictions about plasma-liquid systems, finer scale simulations and/or new experimental techniques must be used to elucidate the near-surface gas phase electron dynamics.

Keywords: plasma-liquid interface, DC discharge with water anode, multiphysics simulation

(Some figures may appear in colour only in the online journal)

1. Introduction

In the low-temperature plasma community there is a burgeoning interest in the study of plasma-liquid systems for both basic and applied research purposes. Applications stemming from the interactions of plasmas and liquids include biomedicine and biological disinfection [3–8], chemical disinfection [9–11], and agricultural uses [12, 13]. To most effectively utilize plasma-liquid systems requires a fundamental knowledge of their behavior; many researchers are now actively contributing to that knowledge through both experimental [1–2, 14–19] and modelling efforts [20–23]. Though much progress has been made, there is still much that is unknown, particularly in the interfacial region where the plasma meets the liquid. For instance, little is really known about how electrons are transported across the interface. Most studies in the literature consider solvation of electrons generated in the aqueous bulk by radiolysis [24, 25]. A highly energetic electron is ejected from the solvent molecule and is initially delocalized in the solvent's conduction band. Eventually the electron is localized in a solvent trap and is electronically relaxed. The electron relaxation is accompanied by orientation of the solvent molecules to solvate the rapidly changing charge distribution [24]. While this qualitatively explains the behavior of several eV electrons generated in the liquid bulk, researchers are keen to learn what additional physiochemical effects might be associated with electron transport across an interface. Rumbach *et al* [1] used absorption spectroscopy to detect the presence of solvated electrons in the surface region with an estimated penetration depth of 2.5 nm. A molecular dynamics study indicates that electrons at the surface of water only have about 10% of their density protruding into the vapor phase, suggesting that their behavior should be much more characteristic of a fully hydrated as opposed to a half-hydrated species [26]. These studies help elucidate the character of the liquid phase side of the interface. However, little work has been done to understand the electron behavior on the gas phase side of the interface. Common gas discharge modelling parameters like the surface loss coefficient for electrons are unknown for the gas–liquid interface. To date plasma-liquid models have assumed a surface loss coefficient of unity [21, 23], however, there is no known molecular scale simulations or experimental measurements to indicate that this assumption should be true.

The modelling work here explores consequences of the above assumption and the uncertainty in electron dynamics on the gas phase side of the interface. To do this, a simple model 1D DC Argon discharge with a water anode is used. The purpose of the work is not to make definitive predictions about the behavior at the plasma-liquid interface but rather to present a range of results that may encompass the true physical behavior. Additionally, the authors hope that the research presented here may motivate deeper studies of the gas-phase side of the interface, whether it be through *ab initio* calculations or experimental techniques.

For this paper, both kinetic and thermodynamic descriptions of the electron density at the interface are considered. A description of the 1D fully-coupled plasma-liquid model is given in section 2. In section 3 it is shown that by varying the interfacial electron surface loss coefficient in the kinetic description or a Henry's law like coefficient in the thermodynamic description, the electron density on the gas phase side of the interface can be changed by orders of magnitude. Moreover, if electrons coming from the bulk are not absorbed at the interface, they become thermalized through non-recombinatory collisions. Conclusions and future work are described in section 4. A brief description of the novel code used to in appendix.

2. Model description

The fully coupled 1D plasma liquid model is implemented in a code developed by the authors. The code, which is open source and free to use (`github.com/lindsayad/zapdos`), is described very briefly in appendix. In the model, a DC atmospheric pressure argon discharge impinges on a very thin water layer. The powered electrode is biased negatively, making it the cathode. From the plasma's perspective, the water surface is the anode. Only elastic collisions, ground state ionization, and ground state excitation are considered. The model governing equations are described below. Continuity equations based on the drift-diffusion approximation are solved for the electrons and ions:

$$\frac{\partial n_i}{\partial t} + \nabla \cdot \vec{\Gamma}_i = S_{\text{iz}} \tag{1}$$

$$\frac{\partial n_e}{\partial t} + \nabla \cdot \vec{\Gamma}_e = S_{\text{iz}} \tag{2}$$

$$\vec{\Gamma}_i = \mu_i \vec{E} n_i - D_i \nabla n_i \tag{3}$$

$$\vec{\Gamma}_e = -\mu_e \vec{E} n_e - D_e \nabla n_e \tag{4}$$

$$S_{\text{iz}} = \alpha_{\text{iz}} |\vec{\Gamma}_e| \tag{5}$$

where μ is the mobility, D the diffusivity, α_{iz} the Townsend ionization coefficient, Γ the species flux, S_{iz} the ionization source term, n the species density, and $\vec{E}$ the electric field, equal to ∇V where V is the potential. Poisson's equation is solved for the potential:

$$-\nabla^2 V = \frac{e(n_i - n_e)}{\epsilon_0} \tag{6}$$

where e is the Coulombic charge and ϵ_0 is the permittivity of free space. The equation for the electron energy is:

$$\frac{\partial (n_e \epsilon)}{\partial t} + \nabla \cdot \vec{\Gamma}_\epsilon = -e\vec{\Gamma}_e \cdot \vec{E} - |\vec{\Gamma}_e| \left(\alpha_{\text{iz}} \epsilon_{\text{iz}} + \alpha_{\text{ex}} \epsilon_{\text{ex}} + 3 \frac{m_e}{m_i} \alpha_{\text{el}} T_e \right) \tag{7}$$

$$\vec{\Gamma}_\epsilon = \frac{5}{3} \epsilon \vec{\Gamma}_e - \frac{5}{3} n_e D_e \nabla \epsilon \tag{8}$$

where ϵ is the mean electron energy, ϵ_{iz} the electron energy lost in an ionization collision, α_{ex} the Townsend excitation coefficient, ϵ_{ex} the electron energy lost in an excitation collision, m_i and m_e the ion and electron masses respectively,

$\alpha_{\rm el}$ the Townsend elastic collision coefficient, and T_e the electron temperature, equal to $\frac{2}{3}\epsilon$.

Plasma boundary conditions at the cathode are based on the work in [27] and [28]. For ions, electrons, and the electron energy, the conditions are respectively:

$$\vec{\Gamma}_i \cdot \vec{n} = \frac{1-r_{\rm i}}{1+r_{\rm i}}\left((2a_i-1)\mu_i\vec{E}\cdot\vec{n}n_i + \frac{1}{2}v_{{\rm th},i}n_i\right) \tag{9}$$

$$\vec{\Gamma}_e \cdot \vec{n} = \frac{1-r_{\rm dens}}{1+r_{\rm dens}}\left(-(2a_e-1)\mu_e\vec{E}\cdot\vec{n}(n_e-n_\gamma) + \frac{1}{2}v_{{\rm th},e}(n_e-n_\gamma)\right) - (1-a_e)\gamma_p\vec{\Gamma}_p\cdot\vec{n} \tag{10}$$

$$\vec{\Gamma}_\epsilon \cdot \vec{n} = \frac{1-r_{\rm en}}{1+r_{\rm en}}\left(-(2a_e-1)\frac{5}{3}\mu_e\vec{E}\cdot\vec{n}(n_e\epsilon-n_\gamma\epsilon_\gamma) + \frac{5}{6}v_{{\rm th},e}(n_e\epsilon-n_\gamma\epsilon_\gamma)\right) - \frac{5}{3}\epsilon_\gamma(1-a_e)\gamma_p\vec{\Gamma}_p\cdot\vec{n} \tag{11}$$

where $r_{\rm i}$, $r_{\rm dens}$, $r_{\rm en}$ are the boundary reflection coefficients for ions, electrons, and electron energy respectively (more discussion on $r_{\rm en}$ shortly), γ_p is the secondary electron emission coefficient, ϵ_γ is the energy of the secondary electrons, $\vec{n}$ is the outward facing normal vector, and:

$$a_k = \begin{cases} 1, & {\rm sgn}_k\mu_k\vec{E}\cdot\vec{n} > 0 \\ 0, & {\rm sgn}_k\mu_k\vec{E}\cdot\vec{n} \leqslant 0 \end{cases} \tag{12}$$

$$v_{{\rm th},k} = \sqrt{\frac{8T_k}{\pi m_k}} \tag{13}$$

$$n_\gamma = (1-a_e)\frac{\gamma_p\vec{\Gamma}_p\cdot\vec{n}}{\mu_e\vec{E}\cdot\vec{n}} \tag{14}$$

where $v_{{\rm th},k}$ is the thermal velocity of species k and n_γ is the density of secondary electrons. All r_k's are set to zero at the cathode. At the interface of the plasma with the liquid phase, the ion boundary condition is the same as for the cathode with $r_{\rm i} = 0$. For electrons in the gas phase two formulations are considered. The first is the kinetic formulation given by equation (10) where $r_{\rm dens}$ is variable. The second is a thermodynamic formulation analogous to Henry's law where the ratio of the liquid phase electron density to the gas phase electron density is specified by a variable H (equivalent to a Henry's law coefficient):

$$Hn_{e,g} = n_{e,l} \tag{15}$$

The electron energy interfacial condition is the kinetic one, see equation (11). Though $r_{\rm dens}$ (or H for the thermodynamic electron BC) at the interface is varied in the results that follow, $r_{\rm en}$ is held constant at 0 for most simulations. This is done for the following physical reasoning. Electrons can either pass freely into the liquid phase, carrying their energy with them, or they can be reflected. If they are reflected, then it is reasonable to expect these electrons to lose their energy in surface collisions such as vibrational excitation of H_2O until they are incorporated into the liquid. Thus though some electrons coming from the bulk may be reflected, it may be reasonable to assume that all the electron energy coming from the bulk is absorbed by the interface. However, in the interest of covering all realms of possibility (perhaps most electron collisions at the interface are low-loss elastic collisions for example), a study is conducted in which the amount of energy absorbed/reflected by the interface is varied. This is done by changing $\gamma_{\rm en}$. While $\gamma_{\rm dens}$ and $\gamma_{\rm en}$ are independent parameters in this model, in reality they are likely interrelated. Future work like that described at the end of section 3 can hopefully elucidate the relationship between the two parameters. Note that in the plots and discussion to follow, the surface loss coefficients $\gamma_{\rm dens}$ and $\gamma_{\rm en}$ will often be used instead of the reflection coefficients $r_{\rm dens}$ and $r_{\rm en}$. The relationship between surface loss and reflection coefficients is simply $\gamma_k = 1 - r_k$.

Table 1. Plasma liquid simulation input parameters.

Parameter	Value
Gas	Argon
Pressure	1 atm
γ_p	0.15
A	$5.02 \cdot 10^{-7}$ m^2
R	$10^6\,\Omega$
$V_{\rm source}$	1.25 kV
Gas domain	1 mm
Liquid domain	100 nm
ϵ_γ	3 eV
T_i	300 K

Table 2. Plasma liquid simulation input parameters.

Coefficient	Value	Source
μ_e	Variable	[31]
D_e	Variable	[31]
μ_i	$3.52 \cdot 10^{-4}$ m^2 s^{-1} V^{-1}	[33]
D_i	$5.26 \cdot 10^{-6}$ m^2 s^{-1}	[33]
$\alpha_{\rm iz}$	Variable	[31]
$\alpha_{\rm ex}$	Variable	[31]
$\alpha_{\rm el}$	Variable	[31]
$\epsilon_{\rm iz}$	15.76 eV	[30]
$\epsilon_{\rm ex}$	11.5 eV	[30]

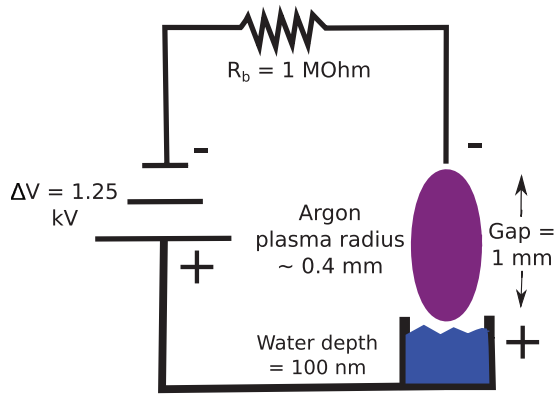

Figure 1. Circuit schematic of coupled plasma liquid system. Note that diagram is not to scale.

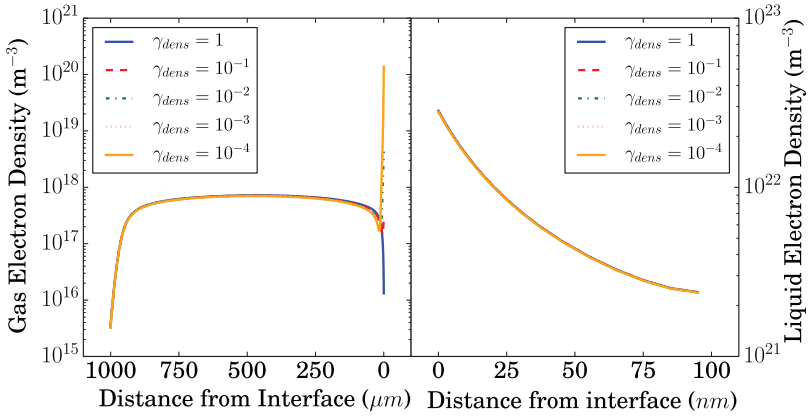

Figure 2. Electron density as a function of the interfacial surface loss coefficient.

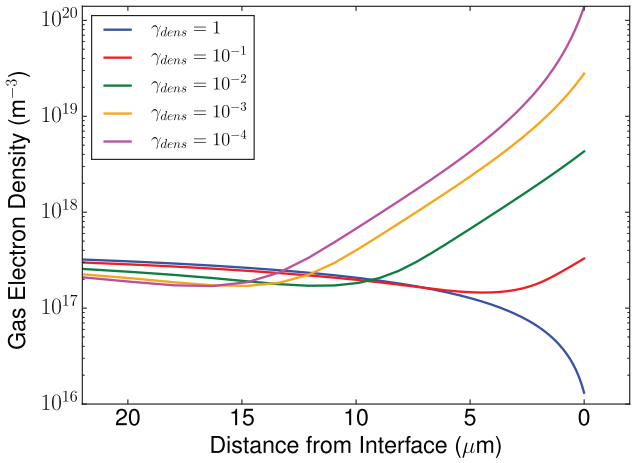

Figure 3. Electron density as a function of the interfacial surface loss coefficient. Final 20 μm of the gas phase before the interface.

The liquid phase electron density interfacial condition is given simply by the continuity of flux. At the bottom of the liquid, electrons are assumed to recombine or flow out at a rate equivalent to the advective flux.

For potential conditions, V is set to zero at the end of the liquid domain. At the cathode, Kirchoff's voltage law for a circuit including a ballast resistor yields:

$$V_{\text{source}} + V_{\text{cathode}} = (e\vec{\Gamma}_i - e\vec{\Gamma}_e)AR \tag{16}$$

where A is the cross-sectional area of the plasma and R is the ballast resistance.

Gas phase electron coefficients were calculated in the following way: argon ionization, excitation, and elastic collision cross sections were taken from the Phelps database [29] at [30]. Then using the open source Boltzmann solver Bolos [31] based on the work of Hagelaar [32] electron energy distribution functions were calculated for 200 electric field points between 10^3 and 10^7 V m^{-1}. Then for each distribution function, μ_e, D_e, ϵ, and the necessary electron collision rate coefficients were calculated as defined by [32]. Transport and rate cofficients were tabulated against the mean energy. These lookup-tables were then referenced during solution of the fluid equations. The details of the inputs for the fluid simulations are given in tables 1 and 2 and figure 1. Mesh sizes for the simulations were typically around 200 elements with most elements located in the cathode and interfacial regions. Each individual simulation took between 12 and 60 s to run.

3. Results and discussion

Figure 2 shows the electron density in both the gas and liquid phases as a function of the interfacial surface loss coefficient. The cathode and bulk profiles are unaffected by changing γ_{dens}. However, as one might expect, decreasing the surface loss coefficient leads to a build-up of electrons on the gas phase side of the interface, seen more clearly in figure 3. Similar behavior can be achieved by decreasing the H coefficient in equation (15); the results are shown in figures 4 and 5. In order to observe anode characteristics akin to those for a plasma in contact with a metallic electrode ($\gamma_{\text{dens}} = 1$), H must be on the order of 10^6. This is on the same order of magnitude as Henry's law coefficients for H_2O_2 and HNO_3, both very hydrophilic species. If H is reduced to 10^4, the gas phase electron density near the interface increases by an order of magnitude. If H is further reduced to 10^2, only slightly less hydrophilic than OH, then the gas phase interfacial density rockets up to three orders of magnitude greater than the metallic anode base case. Decreasing H further only continues the trend.

Despite the dramatic functional dependence of the gas phase electron density in the anode, the liquid phase electron density profile remains unchanged as γ_{dens} is varied. The reason for this can be seen by looking at figure 6. Like the liquid phase electron density profile, the potential drop across the plasma-liquid system is unaffected by changing γ_{dens}. This means that the system DC current is also unaffected, roughly 1000 Amps m^{-2} for all simulation cases. Away from the cathode, all the current is carried by electrons, thus the electron current at the interface between the gas and liquid must also remain unchanged as γ_{dens} is varied. With the liquid phase electron input thus unaffected by γ_{dens}, the liquid phase electron density profile remains constant. Varying γ_{dens} does change the potential and electric field profiles near the interface; this is shown in figure 7. From the low reflection to high reflection extremes, the interfacial electric field increases by about a factor of seven.

As with the electron density, the cathode and bulk electron temperature profiles in figure 8 do not change as γ_{dens} is varied. However, there is major variation in the anode.

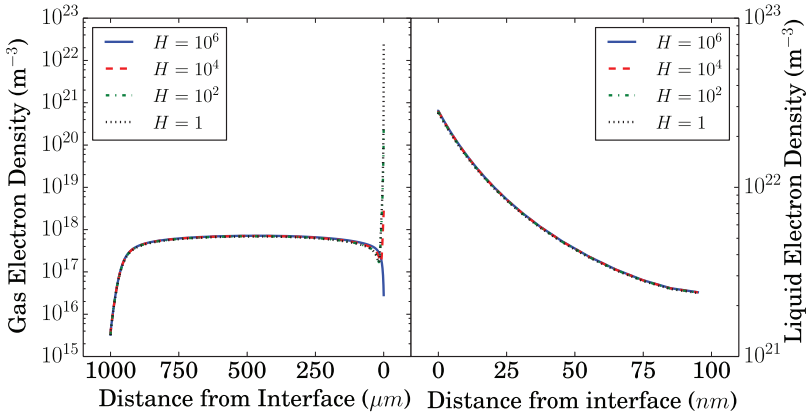

Figure 4. Electron density as a function of H using the thermodynamic boundary condition. Shows same trend as figure 2.

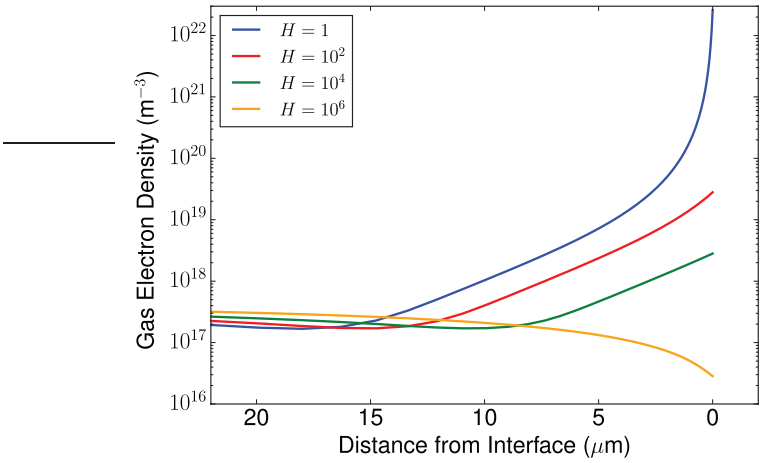

Figure 5. Electron density as a function of H over the last 20 μm of the gas phase. Shows same trend as figure 3.

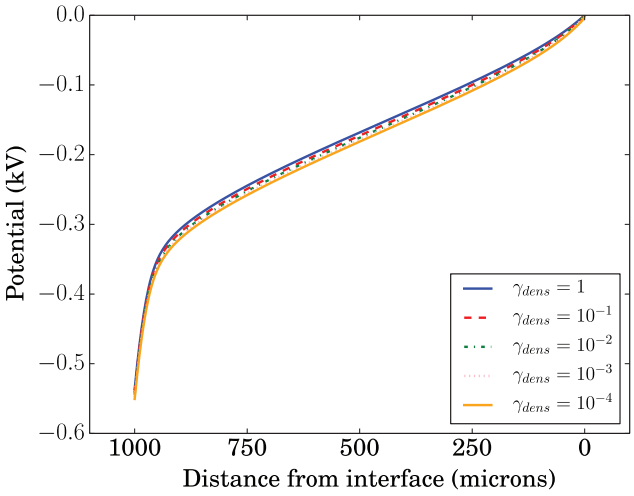

Figure 6. Potential as a function of the interfacial surface loss coefficient.

This variation arises from the assumption described in the model description section that electrons coming from the bulk either carry their energy into the liquid phase upon absorption or else if reflected lose their energy through interfacial surface collisions. The greater the reflection, the lower the average energy of electrons near the interface because of non-recombinatory surface collisions. This is what is observed in figure 8. This trend in electron energy also explains the slight variation in anode ion density profiles seen in figure 9. Lower electron mean energy near the interface means a smaller fraction of electrons with sufficient energy to create ionization and a smaller Townsend ionization coefficient. Because in this model ionization is proportional to the electron flux magnitude and because the electron flux magnitude is constant with respecto to γ_{dens}, the decrease in α_{iz} corresponds to a decrease in the rate of ionization. Hence the ion density rises to its bulk value farther from the anode for decreasing γ_{dens}.

The physically correct boundary condition for the electron energy at the interface is unknown. However, we can vary the amount of electron energy that is absorbed/reflected at the interface and see whether that affects the most important result of the above figures: that interfacial electron density increases significantly as the electron surface loss coefficient is decreased. Figure 10 shows the effect of varying the amount of energy lost at the interface when γ_{dens} is kept constant at 10^{-2}. A couple of trends are notable. The first is that as the energy reflection is increased, e.g. as γ_{en} is decreased, the bulk electron density increases; moreover, instead of retaining a flat profile through the bulk, the electron density increases almost linearly moving from cathode to anode. Additionally, as γ_{en} decreases the jump in electron density at the anode/interface decreases. The combination of these effects results in anodic electron densities that differ by less than a factor of two over

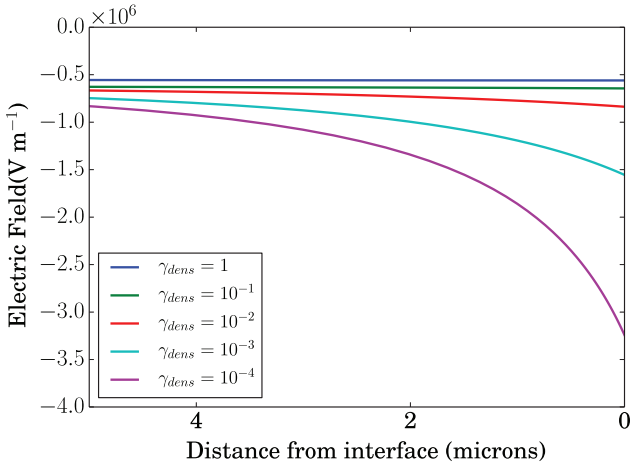

Figure 7. Electric field near the interface as a function of the interfacial surface loss coefficient.

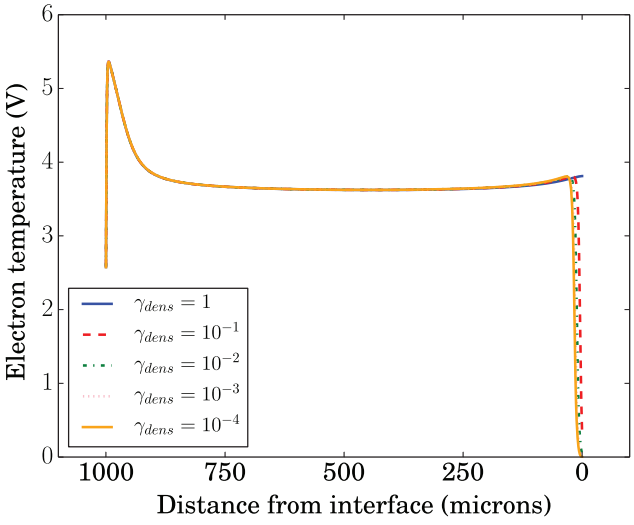

Figure 8. Electron temperature as a function of the interfacial surface loss coefficient.

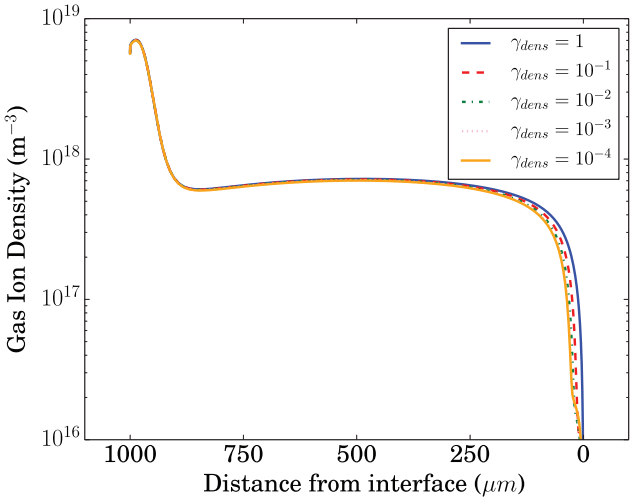

Figure 9. Ion density as a function of the interfacial surface loss coefficient.

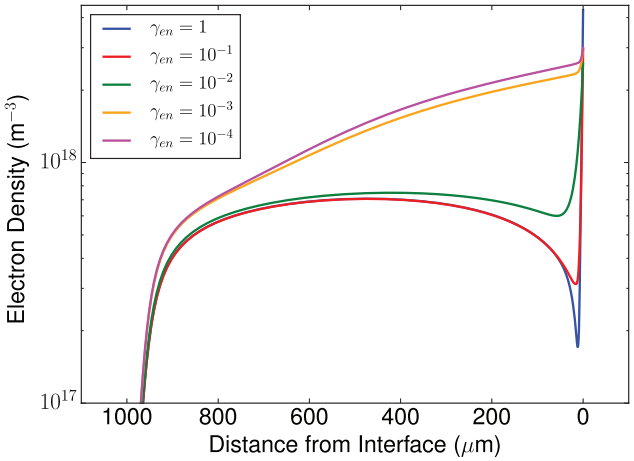

Figure 10. Gas phase electron density as a function of the electron energy interfacial surface loss coefficient. ($\gamma_{dens} = 10^{-2}$ for all cases).

values of γ_{en} that span four orders of magnitude. Moreover, no matter the value of γ_{en}, the anodic electron density with $\gamma_{dens} = 10^{-2}$ is over an order of magnitude higher than if the surface loss coefficients for electrons is set to unity. Thus, we conclude that the important result of increasing anodic electron density with decreasing γ_{dens} is relatively insensitive to the choice of γ_{en}; e.g. without knowing how to properly handle the electron energy boundary condition at the interface, we can still reasonably conclude that a decreasing surface loss coefficient will significantly increase the density of gas phase electron at the interface. The effect of varying γ_{en} on the electron temperature gas phase profile is shown in figure 11. Changes in the cathode and bulk profiles are minimal. However, as one might intuitively expect, increasing energy reflection increases the anodic electron temperature. An increase in electron temperature from the bulk to the anode (observed for $\gamma_{en} = 10^{-4}$) is more consistent with high current atmospheric argon PIC simulations [34].

These trends in the anode electron density and electron temperature at the anode could play an important role in more complex models that consider evaporation of H_2O and dilute aqueous species. The rates of reactions of electrons with these species will depend strongly on the electron density and the electron energy distribution. Different energy distributions might favor vibrational excitation of H_2O or dissociative attachment and the production of electronegative plasma species like O^- and OH^-. The near interface gas chemistry will of course couple back into the liquid phase chemistry. Future work with more complex models will investigate how changing γ_{dens} and γ_{en} affects plasma and liquid chemistry. However, in order to limit the scope of possible results and increase the predictive capability of such models, there must be more certainty in interfacial parameters like γ_{dens} and in the interfacial energy dynamics (represented in this work by γ_{en}. Determination of such characteristics will likely require finer scale simulations (molecular dynamics for instance) and/or new experimental diagnostics that are capable of probing near-interface gas dynamics.

It should be noted that we explored the effect of changing the cathode secondary electron emission coefficient (γ_p). Varying γ_p between 0.05 and 0.3 resulted in an increase in bulk plasma density of about 10%, corresponding to a decrease in the lumped resistivity of the plasma-liquid system. The

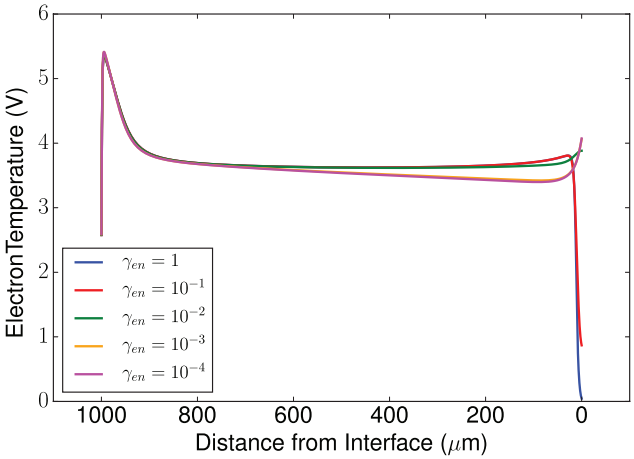

Figure 11. Gas phase electron temperature as a function of the electron energy interfacial surface loss coefficient. ($\gamma_{\text{dens}} = 10^{-2}$ for all cases).

qualitative behavior at the plasma-liquid interface discussed above was unaffected by varying γ_p.

4. Conclusions and future work

In this work it is found that varying the electron surface loss coefficient at the plasma-liquid interface can have significant impacts on both the electron density and electron energy near-interface characteristics. Future work will investigate how these variations could impact plasma chemistry arising from the interaction of the near-interface gas electrons with volatile chemical species coming from the liquid phase. Additionally the model will be expanded to multiple dimensions in the hopes of reproducing the spreading of discharges over the liquid surface as a function of pre-existing ionic concentrations [1]. Modification of solution parameters like the conductivity and pH by the plasma and its experimentally demonstrated feedback (see [35]) into discharge properties will also be considered. Finer scale molecular simulations and/or experiments must be conducted in order to understand the true physical behavior of electrons in the gas near the interface and to accurately determine fluid modelling parameters like γ_{dens}. We hope to expand modelling efforts to various other types of atmospheric discharges including dielectric barrier and surface wave that we can validate against using our own experimental systems. Additionally, interaction of plasmas with liquids other water may also be considered.

Acknowledgments

The authors acknowledge support from the United States Department of Energy, Office of Fusion Science Plasma Science Center and from the National Science Foundation. Thanks to E Kawamura for providing PIC simulation results that helped us in validation of the fluid model implementation. Thanks to R Gopalakrishnan for his literature search of aqueous reactions, rate constants, and transport coefficients. Finally, a very large thanks to the Moose team for all the help along the way in building Zapdos into a successful code.

Appendix. Zapdos code description

Zapdos is built on top of the multiphysics object-oriented simulation environment (MOOSE) [36] and libMesh [37] codes. MOOSE employs finite element methods (continuous Galerkin, discontinuous Galerkin, or a combination) to solve fully coupled (or segregated through the use of MultiApps) systems of partial differential equations (PDEs). After using FEM to discretize the governing equations, MOOSE interfaces with the code PetSc [38] to solve the non-linear system of equations via Newton's method globalized through a line search.

Zapdos partitions governing equation terms into individual pieces called kernels. Each kernel contains the residual (simply the term cast in weak form) and the corresponding Jacobian statements. Consider the drift flux term in charged particle continuity equations: $\nabla \cdot (-\text{sgn}(q)\mu\nabla V)$. After casting into the weak form and taking the volume term, the corresponding Zapdos code looks like:

```
Real EFieldAdvection::computeQpResidual()
{
  return _mu[_qp] * _sign[_qp] * std::exp(_u[_qp]) * -_grad_potential[_qp] * -
    _grad_test[_i][_qp];
}
Real EFieldAdvection::computeQpJacobian()
{
  return _mu[_qp] * _sign[_qp] * std::exp(_u[_qp]) * _phi[_j][_qp] * -
    _grad_potential[_qp] * -_grad_test[_i][_qp];
}
Real EFieldAdvection::computeQpOffDiagJacobian(unsigned int jvar)
{
  if (jvar == _potential_id)
    return _mu[_qp] * _sign[_qp] * std::exp(_u[_qp]) * -_grad_phi[_j][_qp] * -
      _grad_test[_i][_qp];
  else
    return 0.;
}
```

where _u is the solution variable that the kernel is applied to (could be any ion species or electron), _phi and _test represent finite element shape functions (_phi = _test in all cases if using the same order and family of shape functions for all solution variables), and _qp represent the positions of quadrature points. By splitting governing equations in this way into individual terms/kernels, code reproduction is kept at a minimum; analagous terms can be used in many different settings. Material properties like mobilty and diffusivity are defined in a materials file separated from the kernel code. Material properties can be defined as constants, as functions of the solution variables, or as properties to be read from look-up tables. Through MOOSE, Zapdos provides an interface for linear, bilinear, and spline interpolation of material properties. Boundary conditions are available in 'Nodal' and 'Integrated' flavors. Nodal boundary conditions are dirichlet like conditions that are enforced strongly. Integrated boundary conditions are cast in the weak form and often arise from performing integration by parts on divergence terms in the governing equations.

At the time of writing Zapdos has the necessary kernels and boundary conditions for solving gas phase DC discharge fluid models as well as conventional convection-diffusion-reaction equations for dilute species in a fluid. We are also working on implementing RF plasma simulation capabilities (for capacitively coupled plasmas this will only require slight modification of some boundary conditions; inductively coupled plasmas will require a little more work). Anyone interested in contributing to and extending the code is encouraged to contact the authors or fork the repository at `github.com/lindsayad/zapdos`. The MOOSE web-site, `mooseframework.org`, is also a great reference.

References

[1] Rumbach P, Bartels D M, Mohan Sankaran R and Go D B 2015 The solvation of electrons by an atmospheric-pressure plasma *Nat. Commun.* **6** 7248

[2] Rumbach P, Bartels D M, Mohan Sankaran R and Go D B 2015 The effect of air on solvated electron chemistry at a plasma/liquid interface *J. Phys. D: Appl. Phys.* **48** 424001

[3] Kong M G, Kroesen G, Morfill G, Nosenko T, Shimizu T, van Dijk J and Zimmermann J L 2009 Plasma medicine: an introductory review *New J. Phys.* **11** 115012

[4] Laroussi M 2009 Low-temperature plasmas for medicine? *IEEE Trans. Plasma Sci.* **37** 714–25

[5] Shimizu K, Fukunaga H and Blajan M 2014 Biomedical applications of atmospheric microplasma *Curr. Appl. Phys.* **14** 154–61

[6] von Woedtke Th, Metelmann H-R and Weltmann K-D 2014 Clinical plasma medicine: state and perspectives of *in vivo* application of cold atmospheric plasma *Contrib. Plasma Phys.* **54** 104–17

[7] von Woedtke Th, Reuter S, Masur K and Weltmann K-D 2013 Plasmas for medicine *Phys. Rep.* **530** 291–320

[8] Joubert V, Cheype C, Bonnet J, Packan D, Garnier J-P, Teissié J and Blanckaert V 2013 Inactivation of *Bacillus* subtilis var. niger of both spore and vegetative forms by means of corona discharges applied in water *Water Res.* **47** 1381–9

[9] Johnson D C, Dandy D S and Shamamian V A 2006 Development of a tubular high-density plasma reactor for water treatment *Water Res.* **40** 311–22

[10] Locke B R, Sato M, Sunka P, Hoffmann M R and Chang J-S 2006 Electrohydraulic discharge and nonthermal plasma for water treatment *Ind. Eng. Chem. Res.* **45** 882–905

[11] Theron J, Walker J A and Cloete T E 2008 Nanotechnology and water treatment: applications and emerging opportunities *Crit. Rev. Microbiol.* **34** 43–69

[12] Park D P, Davis K, Gilani S, Alonzo C-A, Dobrynin D, Friedman G, Fridman A, Rabinovich A and Fridman G 2013 Reactive nitrogen species produced in water by non-equilibrium plasma increase plant growth rate and nutritional yield *Curr. Appl. Phys.* **13** S19–29

[13] Lindsay A, Byrns B, King W, Andhvarapou A, Fields J, Knappe D, Fonteno W and Shannon S 2014 Fertilization of radishes, tomatoes, and marigolds using a large-volume atmospheric glow discharge *Plasma Chem. Plasma Process.* **34** 1271–90

[14] Lukes P, Dolezalova E, Sisrova I and Clupek M 2014 Aqueous-phase chemistry and bactericidal effects from an air discharge plasma in contact with water: evidence for the formation of peroxynitrite through a pseudo-second-order post-discharge reaction of H_2O_2 and HNO_2 *Plasma Sources Sci. Technol.* **23** 015019

[15] Bruggeman P, Schram D, González M Á, Rego R, Kong M G and Leys C 2009 Characterization of a direct dc-excited discharge in water by optical emission spectroscopy *Plasma Sources Sci. Technol.* **18** 025017

[16] Pavlovich M J, Chang H-W, Sakiyama Y, Clark D S and Graves D B 2013 Ozone correlates with antibacterial effects from indirect air dielectric barrier discharge treatment of water *J. Phys. D: Appl. Phys.* **46** 145202

[17] Traylor M J, Pavlovich M J, Karim S, Hait P, Sakiyama Y, Clark D S and Graves D B 2011 Long-term antibacterial efficacy of air plasma-activated water *J. Phys. D: Appl. Phys.* **44** 472001

[18] Yagi I, Ono R, Oda T and Takaki K 2015 Two-dimensional lif measurements of humidity and oh density resulting from evaporated water from a wet surface in plasma for medical use *Plasma Sources Sci. Technol.* **24** 015002

[19] Bruggeman P, Liu J, Degroote J, Kong M G, Vierendeels J and Leys C 2008 DC excited glow discharges in atmospheric pressure air in pin-to-water electrode systems *J. Phys. D: Appl. Phys.* **41** 215201

[20] Babaeva N Yu, Tian W and Kushner M J 2014 The interaction between plasma filaments in dielectric barrier discharges and liquid covered wounds: electric fields delivered to model platelets and cells *J. Phys. D: Appl. Phys.* **47** 235201

[21] Tian W and Kushner M J 2014 Atmospheric pressure dielectric barrier discharges interacting with liquid covered tissue *J. Phys. D: Appl. Phys.* **47** 165201

[22] Chen C, Liu D X, Liu Z C, Yang A J, Chen H L, Shama G and Kong M G 2014 A model of plasma-biofilm and plasma-tissue interactions at ambient pressure *Plasma Chem. Plasma Process.* **34** 403–41

[23] Shirafuji T, Nakamura A and Tochikubo F 2014 Numerical simulation of electric double layer in contact with dielectric barrier discharge: effects of ion transport parameters in liquid *Japan. J. Appl. Phys.* **53** 03DG04

[24] Kimura Y, Alfano J C, Walhout P K and Barbara P F 1994 Ultrafast transient absorption spectroscopy of the solvated electron in water *J. Phys. Chem.* **98** 3450–8

[25] Paik D H, Lee I-R, Yang D-S, Baskin J S and Zewail A H 2004 Electrons in finite-sized water cavities: hydration dynamics observed in real time *science* **306** 672–5

[26] Uhlig F, Marsalek O and Jungwirth P 2013 Electron at the surface of water: dehydrated or not? *J. Phys. Chem. Lett.* **4** 338–43

[27] Hagelaar G J M, De Hoog F J and Kroesen G M W 2000 Boundary conditions in fluid models of gas discharges *Phys. Rev.* E **62** 1452–4
[28] Sakiyama Y and Graves D B 2007 Nonthermal atmospheric RF plasma in one-dimensional spherical coordinates: asymmetric sheath structure and the discharge mechanism *J. Appl. Phys.* **101** 073306
[29] Yamabe C, Buckman S J and Phelps A V 1983 Measurement of free–free emission from low-energy-electron collisions with ar *Phys. Rev.* A **27** 1345
[30] http://fr.lxcat.net/home/
[31] Luque A 2016 https://github.com/aluque/bolos
[32] Hagelaar G J M and Pitchford L C 2005 Solving the boltzmann equation to obtain electron transport coefficients and rate coefficients for fluid models *Plasma Sources Sci. Technol.* **14** 722
[33] Richards A D, Thompson B E and Sawin H H 1987 Continuum modeling of argon radio frequency glow discharges *Appl. Phys. Lett.* **50** 492–4
[34] Kawamura E 2016 personal communication
[35] Bruggeman P and Leys C 2009 Non-thermal plasmas in and in contact with liquids *J. Phys. D: Appl. Phys.* **42** 053001
[36] Moose Team at Idaho National Lab 2016 mooseframework.org
[37] http://libmesh.github.io/
[38] PetSc Team at Argonne National Lab 2016 http:/mcs.anl.gov/petsc/